Physics and Imaging in Radiation Oncology 16 (2020) 26–32

Contents lists available at ScienceDirect

Physics and Imaging in Radiation Oncology

journal homepage: www.sciencedirect.com/journal/physics-and-imaging-in-radiation-oncology

Original Research Article

Two-dimensional real-time quality assurance dosimetry system using μ-Al_2O_3:C,Mg radioluminescence films

Luana F. Nascimento [a,*], Dirk Verellen [b], Jo Goossens [b], Lara Struelens [a], Filip Vanhavere [a], Paul Leblans [c], Mark Akselrod [d]

[a] Belgian Nuclear Research Centre, Mol, Belgium
[b] Iridium Kankernetwerk, University of Antwerp, Antwerp, Belgium
[c] Agfa NV, Mortsel, Belgium
[d] Landauer, Stillwater Crystal Growth Division, Stillwater, USA

A B S T R A C T

Background and purpose: There is a continual need for more accurate and effective dosimetric systems for quality assurance (QA) as radiotherapy evolves in complexity. The purpose of this project was to introduce a new system that minimally perturbs the main beam, while assessing its real time 2D dose-rate and field shapes. The system combined reusability, linear dose-rate response, and high spatial and time resolution in a single radiation detection technology that can be applied to surface dose estimation and QA.

Materials and methods: We developed a 2D prototype system consisting of a camera, focusing lenses and short pass filter, placed on the head of a linear accelerator, facing an Al_2O_3:C,Mg radioluminescent film. To check the appropriateness of multi-leaf collimator, stability/reproducibility QA tests were prepared using the treatment planning system: including the routinely used alternating leaves, chair and pyramid checks.

Results: The Al_2O_3:C,Mg film did not perturb the dose vs. depth dose curves determined with a point detector (-0.5% difference). Our results showed a dose-rate linear film response ($R^2 = 0.999$), from 5 to 600 MU/min. Measured output factors agreed with reference data within ~1%, indicating a potential for small field dosimetry. Both chair and pyramid measured profiles were comparable with those obtained with the treatment planning system within 1%. The alternating leaves test showed an average discrepancy in the valleys of 14%.

Conclusions: The prototype demonstrated promising results. It obviated the need for corrections regarding the relative position of the camera, confirming accurate dose-rate delivery and detection of radiation fields.

1. Introduction

Quality assurance (QA) is important to the successful implementation of radiation treatments. The technology to verify dose delivery by direct dose measurement for every beam, every fraction, and every patient is not always practical. Hence, there are numerous solutions to verify the pre-treatment delivery to a phantom [1,2]. However, pre-treatment QA is the least sensitive tool to detect errors out of all control checks in radiation oncology [3], highlighting the need for real-time patient specific QA.

Several authors have proposed solutions to assess real-time patient doses during treatment. Such solutions included diodes [4], metal-oxide semi-conductor field effect transistors [5], organic and inorganic scintillation detectors [6,7], radioluminescent (RL) crystals [8], Cherenkov emission [9], transmission detectors [10] and electronic portal imaging devices [11].

In general, point and 2D scintillators\RL detectors were reliable solutions, but they had some specific differences, such as time/spatial resolution, film homogeneity, quenching, optical scattering, glaring effects and interference from Cherenkov emission [12,13]. Moreover, most dose measurements from these systems presented an integration time of 150 ms when using Electron Multiplying Charge Coupled Device (EMCCD) cameras or a few seconds when using Charge Coupled Device (CCD) cameras, in order to accumulate a good signal-to-noise ratio [14,15]. The primary aim for this study was to present an independent QA tool that combines real-time dose-rate assessment with high spatial resolution. The system consisted of a thin RL film based on Al_2O_3:C,Mg [16] and a digital camera that images the RL signal with intensity proportional to the radiation dose rate and shape.

Our system has a novel method to visualize in real-time the entrance of radiation beams at a phantom or patient surface, with an improved time resolution of 20 ms, using a camera fixed to the head of the linear accelerator (LINAC). This increased time resolution, compared to previous systems, is a clear advantage for treatments involving many small

* Corresponding author.
E-mail address: ldfnasci@sckcen.be (L. F. Nascimento).

https://doi.org/10.1016/j.phro.2020.09.008
Received 6 March 2020; Received in revised form 23 September 2020; Accepted 25 September 2020
Available online 5 October 2020

and irregular multileaf collimator (MLC) fields or segments that are delivered in dynamic mode, such as intensity-modulated radiation therapy (IMRT) and volumetric modulated arc therapy (VMAT). In addition, we present, for the first time, Al_2O_3:C,Mg RL as a suitable material for 2D real time dosimetry. In the following sections, the system's dosimetric experimental validation is described, together with a number of QA tests.

2. Materials and methods

2.1. System setup

The system, referred to from here as ImageDosis, consisted of a flexible RL film based on micro-crystals of Al_2O_3:C,Mg and a digital camera. The film emitted light when exposed to ionizing radiation (Supplementary Fig. S1). The measurements presented in this paper have a field-of-view of 200 mm^2.

We used an EMCCD camera (Raptor), a commercial lens (Fujinon) and a 420 nm Bandpass Filter (Sigma). The camera (640 × 480 pixels) was fixed at the head of the LINAC using a device that allows the camera to be placed at a consistently fixed position, focused on the field isocentre. By using this fixing device, we did not need to correct for positioning differences when changing from one machine to another. The camera was controlled by the μManager software [17] and image processing was done using Fiji [18]. AGFA HealthCare NV, using RL material from Landauer USA, produced the 200 mm^2 sheets. The films were 75 μm thick, composed of 7 μm layer of Al_2O_3:C,Mg powder grains in the polymer binder deposited on a water equivalent substrate of white Polyethylene terephthalate (PET).

We used the Interactive Perspective plugin from Fiji to correct the acquired images for the off-normal to normal angle. The pixels from the images were transformed into a calibrated image space using markers in the phantom and LINAC light field edges, so that each pixel area corresponds to 0.1 mm. When necessary, parts of the image were smoothed by a noise removal filter to remove saturated pixels caused by high-energy scattered photons. The pixel intensity signal used for the dosimetric characterizations of each film consisted of the average RL signal over a specified region of interest subtracted by the average background signal. Background images (around 50) were acquired by averaging images prior and post irradiation at the same sampling rate used for the images acquired during irradiation (one image every 20 ms). The standard deviation (SD) of the background light did not exceed 0.5%.

2.2. Irradiations and tests

We irradiated the films using a TrueBeam Varian (Varian Medical Systems Inc., Palo Alto, CA), with 6 MV photons in flattening filter mode giving dose rates from 5 to 600 monitor units (MU)/min. Square field sizes ranged from 10 to 150 mm^2. The LINAC was calibrated using the NCS report 18 [19] to obtain an equivalence of 1 cGy/1 MU at d_{max} in reference conditions, for a 100 mm^2 field size and a 100 cm source-to-surface distance (SSD). The measurements were performed using a series of PMMA transparent slab phantoms.

The reference data used in this study were obtained using a Semiflex ionization chamber (PTW) at d_{max}. QA checks were planned using the Varian Eclipse v13.6 (Varian Medical Systems Inc., Palo Alto, CA) treatment planning system (TPS) using a dosegrid of 1 mm.

To investigate if the film interferes with the radiation beam, we placed it at the surface of a slab phantom and measured dose vs. depth using an optical fibre prototype [8,20], comparing the results with those obtained when the film is not in front of the 100 mm^2 beam. The fibre was placed both at the centre of the field (x = 0) and out-of-field (x = 60 mm).

For the dosimetric characterization, we performed dose-rate response and output factor measurements for various fields. The dose-rate response was investigated by irradiating films at a 10 mm depth within a PMMA slab phantom with 100 MU and field size of 100 mm^2. The response of the film against dose rate was determined in a region of interest of 20 mm^2. As Varian accelerators do not change the dose per pulse but the number of pulses per unit time, we also performed measurements changing the source-to-surface distance (Supplementary Fig. S2). Next, Output factors were calculated for different square field sizes generated by the jaws, with films irradiated with 100 MU at d_{max}. All measurements were performed at gantry 0° and normalized to the 100 mm^2 reference field.

The capacity to check the stability of the multi-leaf collimator (MLC) and the reproducibility of the gap between leaves was studied by chair, pyramid and alternating leave QA tests [21–23]. The chair field was a 100 mm^2 field containing an irregular shaped MLC forming a chair figure. The alternating leaves test was a 100 mm^2 field that had 5 mm open-closed leaves. The pyramid test had squared MLC fields of 25, 50, 75, 100, and 150 mm^2 with monitor units distributed equally between the different field sizes.

3. Results

3.1. Film perturbation

Measured depth dose curves, at isocenter, with and without the presence of the RL film (Fig. 1a), presented a downward trend after d_{max} at position 16 mm, while the two components followed each other very closely. The measurements resulted in a negligible average perturbation effect (~0.3%), with a maximum measured difference of −0.45%, within 5 mm of the surface (upper image, Fig. 1a). Likewise, for out-of-field measurements (Fig. 1b), the difference between the depth dose curves (without and with film) was −4% within 8 mm of the surface (upper image, Fig. 1b). These results showed that the presence of the film interferes minimally with the measurements from the optical fibre system placed at various depths.

3.2. Dose-rate response

The measured pixel light intensity from squared fields increased with dose-rate (Fig. 2a), being the 10 MU/min image the dullest and 600 MU/min the brightest image. The system's dose rate response (Fig. 2b), translated from pixel light intensities, resulted in a linear line (R^2 = 0.999), with insert image showing also good linearity at the lowest dose-rates.

3.3. Output factors

The real time images (Fig. 3a) from films irradiated with various square fields showed sharp field edges and reasonable uniformity from 100 mm^2 down to 10 mm^2. The measured output factors (Fig. 3b) presented good reproducibility even for the smallest field sizes. The relative standard deviation of the output factors for the measurements was<1.7% (1 SD). It is noteworthy that a good agreement was obtained from the differences in output factors from the films and ionization chamber (upper image, Fig. 3b).

3.4. QA alternating leaves test

All features from the alternating leave test were observed by the images acquired with the film (Fig. 4a), such as the characteristic peaks and valleys, equally spaced in 100 mm^2.

When we compared quantitatively the measured data against the planned test for pixel intensities (normalized to the middle value), the planned data presented deeper valleys (i.e. lower dose below the leaves) relative to the film measurements (Fig. 4b).

The differences in the valleys between planned and film (secondary axis, Fig. 4b) presented an average deviation of 12%, with maximum and minimum differences of 15% and 5% for valley numbers five and

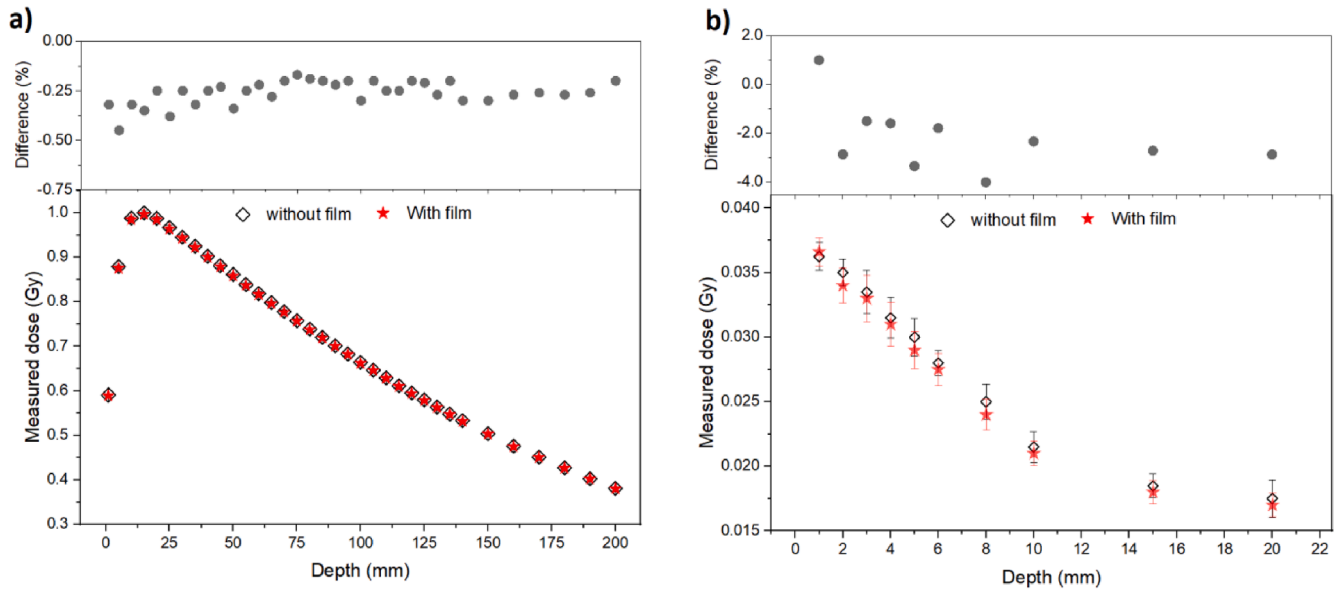

Fig. 1. Measured depth dose curves in a 100 m^2, 6 MV beam where (a) the point optical fibre system is placed at the isocentre of the beam (x = 0 mm) and (b) at the out of field (x = 60 mm, where average energy is ≈100 keV), with and without the RL films placed at the surface of the PMMA plates. Error bars, when visible, are the standard deviation of the measure (1SD). Upper plots presents the difference between the curves (with and without the presence of the film).

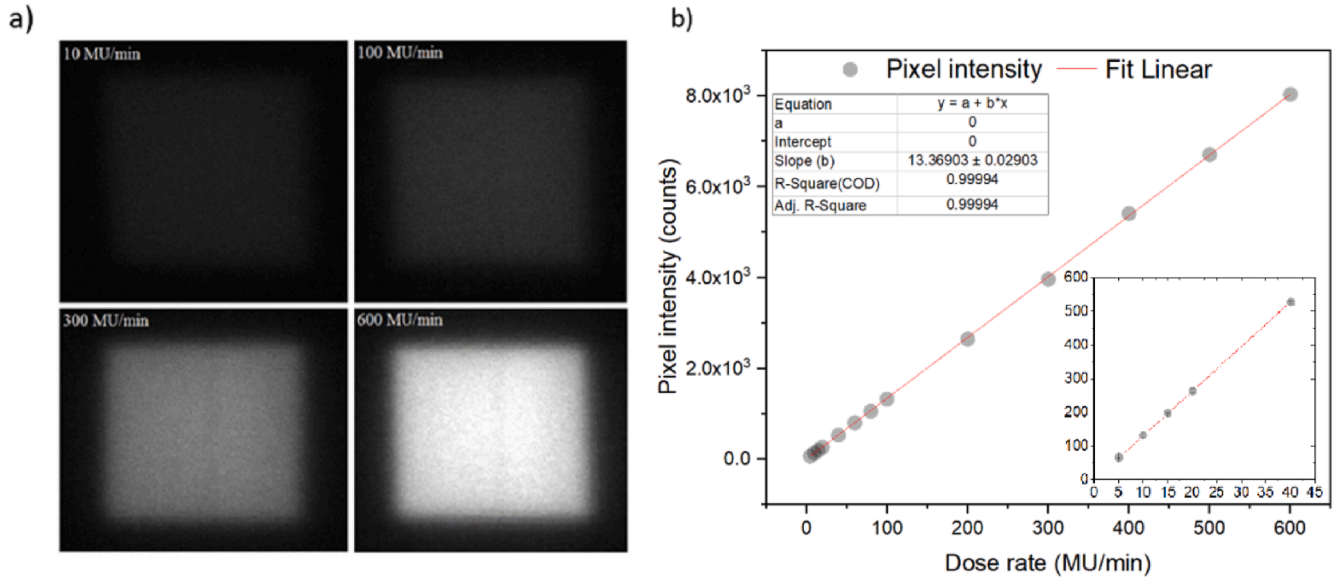

Fig. 2. (a) Example images of 100 mm^2 squared field films irradiated with different dose rates (10, 100, 300 and 600 MU/min) and (b) plotted pixel intensity measurements against LINAC dose rates, from 5 to 600 MU/min. A linear fit shows a R^2 = 0.999 and slope of 13 Counts/(MU*min-1). Insert plot shows the curve from the lowest dose-rates (5 to 40 MU/min). The data points for dose rates above 15 MU/min have standard deviations within 1%, and within 3% for the experimental values of 5, 10 and 15 MU/min. Error bars, where visible, are the standard deviation (1 SD).

nine, from left to right, respectively. The full width at half maximum (FWHM) for the planned was 4.9 mm, while the film presented an average of 6.7 ± 0.2 mm.

3.5. QA chair test

The real time image acquired from the planned chair test (Fig. 5a) outlined different profiles along the crossline and inline fields that correctly resembled a chair. To quantify the accuracy of the image, we chose two crossing lines from the chair image (line 1 and 2, Fig. 5a) and plotted, in Fig. 5b, the film's pixel intensities (normalized to the maximum value) against length (mm), compared to the same lines from the TPS plan.

We observe similar results from measured and planned profiles. The upper graph of Fig. 5b presents the FWHM for the TPS of 74 mm, whilst the film presented an average of 74.2 ± 0.4 mm. For the lower graph, the FWHM for the TPS was 18.7 mm for both profiles, while the film gives 18.8 ± 0.3 mm and 18.8 ± 0.4 mm for the first and second profiles, from left to right, respectively.

The secondary axis from Fig. 5b presents the difference between measured and planned profiles. For line 1, the difference is below 1% for the interval 20 to 80 mm, and below 1.8% for the profile edges (<20 mm and >80 mm). For line 2, the difference is below ±1% for the interval 12 to 35 mm and 70 to 92 mm, and below 2% for the profiles edges (<12 mm and >90 mm).

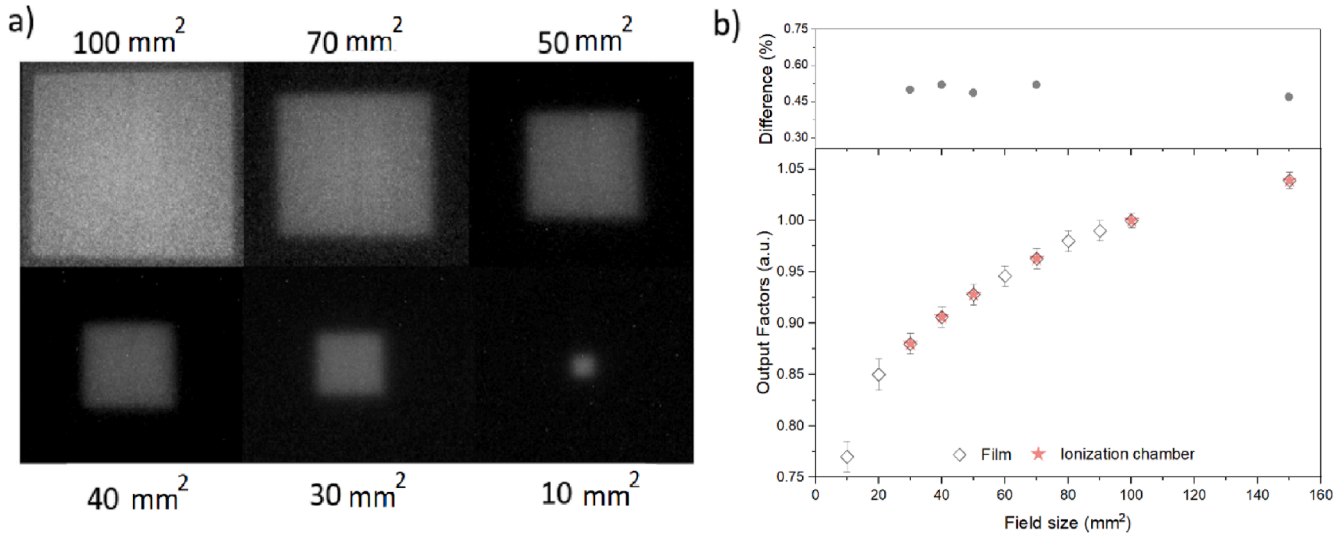

Fig. 3. (a) Various square fields from RL films acquired in real time for different field sizes and (b) output factors against field size calculated from the film and compared with those determined with the Semiflex ionization chamber. Error bars are the standard deviation over the different films acquired with the same acquisition settings. Upper plot is the difference between film and ionization chamber output factors. Good agreement is obtained within 0.5% for field sizes ≥30 mm^2. Uncertainty in the ionization chamber measurements are negligible (<0.5%) and are not presented in the plot.

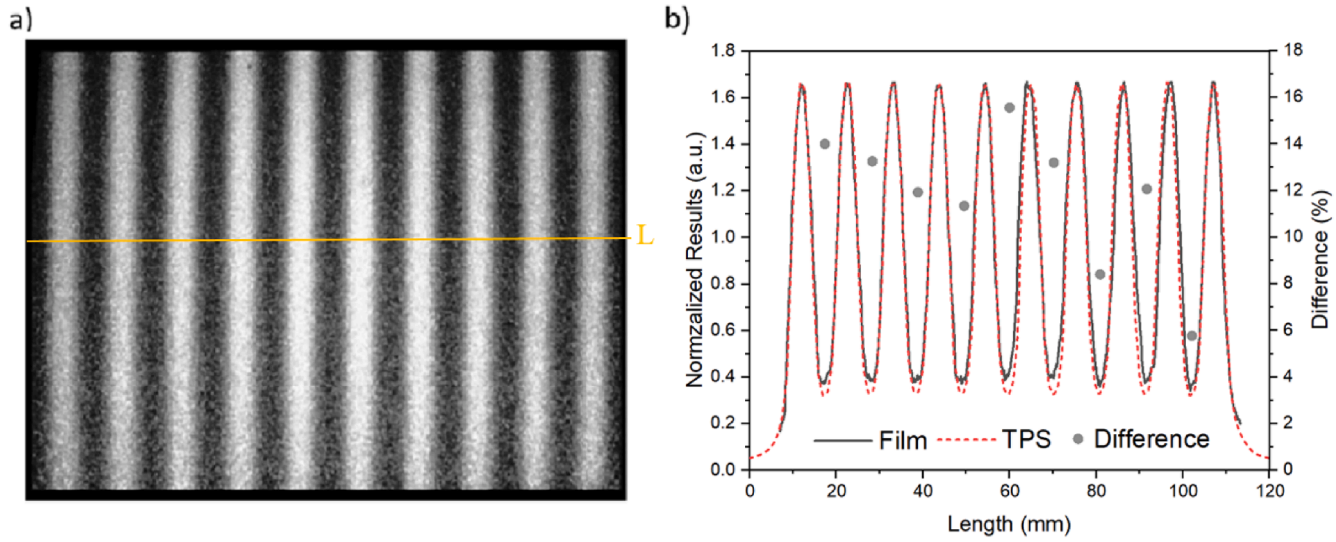

Fig. 4. Alternating leaves of 5 mm in a 100 mm^2 field detected by (a) the RL system and (b) the normalized profile along the centre of the image (line 'L' crossing the image a) in comparison with the profile obtained from the planned TPS test. Secondary axis from the plot is the difference between measured (film) and planned (TPS) profiles.

3.6. QA pyramid test

The superposition of squared profiles acquired with the RL film provided a pyramid-like light distribution image (Fig. 6a). The film's pixel intensities (normalized to the maximum value) against length was compared with the profile from the planned test in the TPS (line 'L' from Fig. 6a, plotted in Fig. 6b). The curves increased smoothly with length to reach the maximum value around 75 mm, decreasing in a mirrored way to reach a minimum at 160 mm. The differences between both curves (upper image, Fig. 6b) were mostly within ±1% for the interval ±120 mm, reaching a maximum of 4% at both extremities.

4. Discussion

We have successfully demonstrated the feasibility of using Al_2O_3:C, Mg for 2D dosimetry in real-time radiotherapy. Real-time beam tracking offers several advantages, for example, the ability to monitor beam position and shapes during treatment delivery. The key findings of the study were: (a) the depth dose curves measured with and without the presence of the film did not present a significant change both at isocenter or out-of-field; (b) the dose-rate response was linear; c) measured output factors showed potential for small field dosimetry; d) measured QA checks were reasonably consistent with TPS tests.

The difference between the curves (Fig. 1a) were within the uncertainty of the optical fibre system (~0.3%) [24]. These results are comparable with the perturbation measured with transmission detectors (MagicPlate and monolithic silicon detector) [25,26], and other systems somewhat similar to ours in concept, such as the GOS scintillator film (-0.6%) [27]. (c)In out-of-field, the difference between the curves (Fig. 1b) did not exceed −4%, which is also comparable with the optical fibre detector accuracy at such low dose (≈10 mG) and energies (≈ 50 keV).

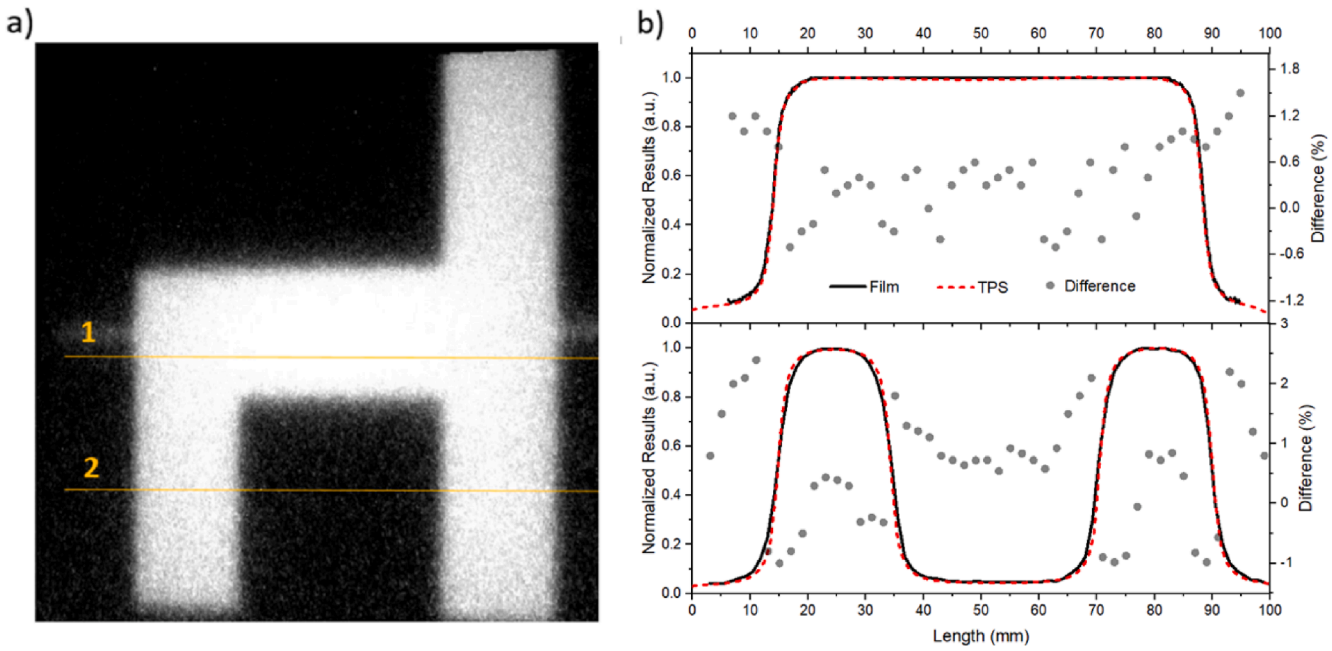

Fig. 5. Chair test in a 100 mm^2 field a) captured by the RL system and b) profile comparison with TPS for line 1 (upper graph) and line 2 (lower graph). Secondary axis from the plots are the differences between measured (film) and planned (TPS) profiles. The average difference for the out of field region between the profiles is 1%.

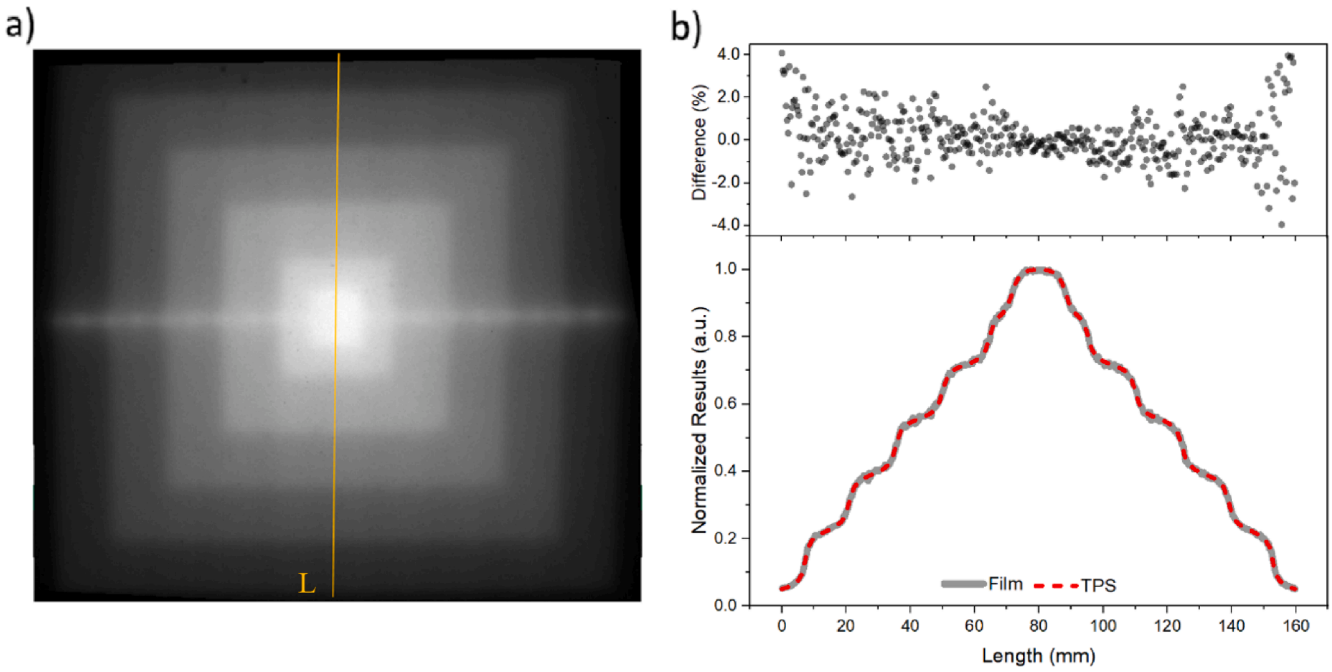

Fig. 6. Pyramid test a) captured by the RL system, with the superposition of various square field sizes and b) profile comparison with TPS for the top-to-bottom line 'L'. Upper plot is the difference between measured (film) and planned (TPS) profiles.

We have presented a good linear dose-rate response ($R^2 = 0.999$). Most of plastic scintillators studies integrate the dose over a specific time span [6], whereas our results are presented in terms of dose-rate. GOS composite materials were linear with absorbed dose [28]. However, a study presenting a similar system to ours (camera + GOS scintillating material) only reported dose-rate measurements from 200 to 600 MU/min [27]. Another promising scintillating material, BCF-12, has low Z_{eff} ~ 6.56 and decay time (3 ns), but a low light yield, which limits its use for low dose and dose rate applications using cameras [29].

Accurate measurement of small radiation fields is a well-known challenge, due to loss in charged particle equilibrium. The potential of Al_2O_3:C point detectors for small field dosimetry was successfully accessed by many authors [30,31]. Several works demonstrated that plastic scintillators measured higher output factors than an ionization chamber, silicon diode and/or radiographic film [32], due to difficulties to correct for the Cherenkov radiation and the differences in the active volumes of the detectors. Our 2D film agreed well (within ≤1%) with reference data (Fig. 3b).

Our system QA checks showed good general agreement with the TPS. The profiles from Fig. 4 presented in detail the alternating peaks and

valleys according to the open and closed leaves. At such small delivered fields, our system had a lower measured resolution, i.e. a larger FWHM consistent with the reported values (6.7 ± 0.2 mm) in this study. A similar issue with lower resolution was also reported for 2D planar and cylindrical diode arrays [33], while other studies presented discrepancies of 20–40% between Monte Carlo simulations, TPS and measurements [34,35]. When we integrated a sequence of 10 images (resulting in a 200 ms integrated image), the signal-to-noise ratio improved and the difference observed in the valleys were 2–3%, with FHWM = 5.5 ± 0.2 mm. It is possible that part of the overresponse observed in the valley region were due to the films material's specific energy dependency for energies below 100 keV [30,36].

Chair and pyramid tests from GafChromic films and ionization chambers were comparable with the profiles measured using our RL system (Figs. 5 and 6) [23]. Lambert et al. [37] presented pyramid fields measured by a plastic scintillator. The dose readings agreed to within 1% with the reference ionization chamber, inside the main field, with no information, however, about the edge region of the pyramid field to account for lower dose resolution. For the chair check, we compared our results with other publications focusing on lateral profile dependence results, as we could not find similar tests. Pönisch et al. [38] showed a series of liquid scintillator measurements for different field sizes. Their results were in good agreement with the dose profile except at the shoulder and tail (not quantified by the authors). Guillot et al. [39] demonstrated that arrays of plastic scintillation detectors could be used for QA in clinics, with step-and-shoot plans.

The main difference between the cited studies and the results presented in our work was that we achieved comparable results with the TPS with images acquired with high time resolution (20 ms) and (crucially) that our films could be used for surface dose assessments, due to their thin characteristics.

Our results demonstrated that there is potential for using a real-time solution based on RL films imaged by a camera to evaluate dose-rate and radiation field shapes. The difference we observed at penumbra and out-of-field can be further investigated and corrected. It is our goal to improve, in the future, the Z_{eff} of the films by adapting the combination of micro-crystal + binder, as we know that smaller crystal size combined with more what equivalent binder implies better water equivalency [20].

Real-time in vivo dosimetry is highly necessary in several applications, for instance, in hypofractionated treatments. An ideal dosimetric system should be able not only to measure dose accurately, but also to detect other sources of discrepancies independently (such as set-up errors). Our system would provide independent safety checks in addition to the existing technologies. ImageDosis will be further developed so in the future radiation therapists/medical physicists could use this as a safety feature to stop treatment if the radiation delivery appears to be incorrect.

In conclusion, we have presented data of a prototype system for ensuring the accurate and safe delivery of radiation in clinical practice. This study differed from other scintillators/RL systems in that the camera is placed at the head of the LINAC, facing the isocenter of the beam and the film. This simplified the need for corrections regarding the relative position of the camera, as it is always fixed in the same position related to the beam. We demonstrated that the films minimally perturb the main beam, confirming accurate dose-rate delivery and detection of radiation field shapes (from jaws and multileaf collimators).

Declaration of Competing Interest

The whole concept of the ImageDosis system was developed in SCK CEN primarily by dr. Luana de Freitas Nascimento. Dr. Mark Akselrod (Landauer Inc.) is a long-time collaborator, his role was to provide dosimetric materials (and help with questions concerning the dosimetric properties of the material he grows), in special, we asked for micro-crystals, much smaller than the ones Landauer Inc. normally uses in their commercial business. Dr. Akselrod also provided the first films we tested, but the homogeneity of the films had to be improved – again, these films are not commercially available. This is when we reached AGFA (Dr. Leblans), as they have a long experience in coating and printing. They agreed to coat Dr. Akselrod's micro-crystals for us. All of these happened in a pure collaborative manner and there are absolutely no competing financial or personal interests at play here.

Acknowledgement

The work presented in this article was partially supported by the Belgian Foundation against Cancer (Grant ID: FAF-C/2016/842; link - https://www.kanker.be/project/team-van-professoren-luana-de-freitas-nascimento-dirk-verellen). Additionally, Luana de Freitas Nascimento would like to thank Dr. Alice Bezett and Prof. Dr. Jordi Vives i Batlle for valuable comments and for proof-reading the manuscript.

Appendix A. Supplementary data

Supplementary data to this article can be found online at https://doi.org/10.1016/j.phro.2020.09.008.

References

[1] Rangaraj D, Yaddanapudi S, Cai J. Transmission detectors are safe and the future for patient-specific QA in radiation therapy. Med Phys 2019;46:1–4. https://doi.org/10.1002/mp.13201.
[2] Bresciani S, Poli M, Miranti A, Maggio A, Di Dia A, Bracco C, et al. Comparison of two different EPID-based solutions performing pretreatment quality assurance: 2D portal dosimetry versus 3D forward projection method. Phys Med 2018;52:65–71. https://doi.org/10.1016/j.ejmp.2018.06.005.
[3] Ford EC, Terezakis S, Souranis A, Harris K, Gay H, Mutic S. Quality control quantification (QCQ): a tool to measure the value of quality control checks in radiation oncology. Int J Radiat Oncol Biol Phys 2012;84:e263–9. https://doi.org/10.1016/j.ijrobp.2012.04.036.
[4] Biasi G, Petasecca M, Guatelli S, Hardcastle N, Carolan M, Perevertaylo V, et al. A novel high-resolution 2D silicon array detector for small field dosimetry with FFF photon beams. Phys. Medica 2018;45:117–26. https://doi.org/10.1016/j.ejmp.2017.12.010.
[5] Van Gellekom MP, Canters RA, Dankers FJ, Loopstra A. van der Steen-Banasik EM, Haverkort MA. In vivo dosimetry in gynecological applications—A feasibility study. Brachytherapy 2018;17:146–53. https://doi.org/10.1016/j.brachy.2017.04.240.
[6] Beaulieu L, Beddar S. Review of plastic and liquid scintillation dosimetry for photon, electron, and proton therapy. Phys Med Biol 2016;61:R305. https://doi.org/10.1088/0031-9155/61/20/R305.
[7] Lecoq P. Development of new scintillators for medical applications. Nucl Instrum Methods Phys Res B 2016;809:130–9. https://doi.org/10.1016/j.nima.2015.08.041.
[8] Nascimento L, Veronese I, Loi G, Mones E, Vanhavere F, Verellen D. Radioluminescence results from an Al2O3: C fiber prototype: 6 MV medical beam. Sens Actuator A Phys 2018;274:1–9. https://doi.org/10.1016/j.sna.2018.03.007.
[9] Spinelli AE, Boschi F. Novel biomedical applications of Cerenkov radiation and radioluminescence imaging. Phys Med 2015;31:120–9. https://doi.org/10.1016/j.ejmp.2014.12.003.
[10] Li T, Wu QJ, Matzen T, Yin FF, O'Daniel JC. Diode-based transmission detector for IMRT delivery monitoring: a validation study. J Appl Clin Med Phys 2016;17:235–44. https://doi.org/10.1120/jacmp.v17i5.6204.
[11] van Elmpt W, Ezzell GA. EPID dosimetry must soon become an essential component of IMRT quality assurance. Controversies in Medical Physics: a Compendium of Point/Counterpoint Debates Volume 2. 2012; 62. https://doi.org/10.1118/1.3213082.
[12] O'Keeffe S, McCarthy D, Woulfe P, Grattan M, Hounsell A, Sporea D, et al. A review of recent advances in optical fibre sensors for in vivo dosimetry during radiotherapy. Br J Radiol 2015;88:20140702. https://doi.org/10.1259/bjr.20140702.
[13] Johnstone CD, Therriault-Proulx F, Beaulieu L, Bazalova-Carter M. Characterization of a plastic scintillating detector for the small animal radiation research platform (SARRP). Med Phys 2019;46:394–404. https://doi.org/10.1002/mp.13283.
[14] Lacroix F, Archambault L, Gingras L, Guillot M, Beddar AS, Beaulieu L. Clinical prototype of a plastic water-equivalent scintillating fiber dosimeter array for QA applications a. Med Phys 2008;35:3682–90. https://doi.org/10.1118/1.2953564.
[15] Archambault L, Briere TM, Pönisch F, Beaulieu L, Kuban DA, Lee A, et al. Toward a real-time in vivo dosimetry system using plastic scintillation detectors. Int J Radiat Oncol Biol Phys 2010;78:280–7. https://doi.org/10.1016/j.ijrobp.2009.11.025.
[16] Akselrod MS, Akselrod AE, Orlov SS, Sanyal S, Underwood TH. Fluorescent aluminum oxide crystals for volumetric optical data storage and imaging

applications. J Fluoresc 2003;13:503–11. https://doi.org/10.1023/B:JOFL.0000008061.71099.55.
[17] Stuurman N, Amdodaj N, Vale R. µManager: open source software for light microscope imaging. Micros Today 2007;15:42–3. https://doi.org/10.1017/S1551929500055541.
[18] Schindelin J, Arganda-Carreras I, Frise E, Kaynig V, Longair M, Pietzsch T, et al. Fiji: an open-source platform for biological-image analysis. Nat Methods 2012;9:676. https://doi.org/10.1038/nmeth.2019.
[19] Stralingsdosimetrie NCV. Code of practice for the absorbed dose determination in high energy photon and electron beams. 2008; http://doi.org/10.25030/ncs-18.
[20] Nascimento L, Vanhavere F, Kodaira S, Kitamura H, Verellen D, De Deene Y. Application of Al2O3: C+ fibre dosimeters for 290 MeV/n carbon therapeutic beam dosimetry. Radiat Phys Chem 2015;115:75–80. https://doi.org/10.1016/j.radphyschem.2015.06.001.
[21] Clivio A, Vanetti E, Rose S, Nicolini G, Belosi MF, Cozzi L, et al. Evaluation of the machine performance check application for TrueBeam linac. Radiat Oncol 2015;10:97. https://doi.org/10.1186/s13014-015-0381-0.
[22] Van Esch A, Bohsung J, Sorvari P, Tenhunen M, Paiusco M, Iori M, et al. Acceptance tests and quality control (QC) procedures for the clinical implementation of intensity modulated radiotherapy (IMRT) using inverse planning and the sliding window technique: experience from five radiotherapy departments. Radiother Oncol 2002;65:53–70. https://doi.org/10.1016/s0167-8140(02)00174-3.
[23] Sathiyan S, Ravikumar M, Varatharaj C, Supe S, Keshava S. IMRT Implementation and patient specific dose verification with film and ion chamber array detectors. Gulf J Oncolog 2010;1:20–7. https://doi.org/10.2478/v10013-009-0009-5.
[24] Nascimento LF. On-line dosimetry for radiotherapy using non-invasive optical fibre sensors with Al2O3:C RL/OSL detector Faculteit Ingenieurswetenschappen en Architectuur. Ghent University. 2015. URL: https://lib.ugent.be/catalog/rug01:002181532.
[25] Alrowaili Z, Lerch M, Petasecca M, Carolan M, Rosenfeld A. Effect of scattered electrons on the 'Magic Plate' transmission array detector response. J Phys Conf Ser 2017;777:012033. https://doi.org/10.1088/1742-6596/777/1/012033.
[26] Utitsarn K, Alrowaili ZA, Stansook N, Petasecca M, Carolan M, Perevertaylo VL, et al. Impact of a monolithic silicon detector operating in transmission mode on clinical photon beams. Phys Med 2017;43:114–9. https://doi.org/10.1016/j.ejmp.2017.10.017.
[27] Jenkins CH, Naczynski DJ, Shu-Jung SY, Xing L. Monitoring external beam radiotherapy using real-time beam visualization. Med Phys 2015;42:5–13. https://doi.org/10.1118/1.4901255.
[28] Glendinning A, Hunt S, Bonnett D. Measurement of the response of Gd2O2S: Tb phosphor to 6 MV x-rays. Phys Med Biol 2001;46:517. https://doi.org/10.1088/0031-9155/46/2/317.
[29] O'Keeffe S, McCarthy D, Woulfe P, Grattan M, Hounsell A, Sporea D, et al. A review of recent advances in optical fibre sensors for in vivo dosimetry during radiotherapy. Brit. J Radiol 2015;88. https://doi.org/10.1259/bjr.20140702.
[30] Tariq M, Gomez C, Riegel AC. Dosimetric impact of placement errors in optically stimulated luminescent in vivo dosimetry in radiotherapy. phiRO 2019;11:63–8. https://doi.org/10.1016/j.phro.2019.08.004.
[31] Ploquin N, Kertzscher G, Vandervoort E, Cygler J, Andersen CE, Francescon P. Use of novel fibre-coupled radioluminescence and RADPOS dosimetry systems for total scatter factor measurements in small fields. Phys Med Biol 2014;60:1. https://doi.org/10.1088/0031-9155/60/1/1.
[32] Chen L, Chen S, Woulfe P, Gillespie S, Viphavakit C, Jiang B, et al. Investigation of YAG: Ce based optical fibre sensor for use in external beam radiotherapy dosimetry. Opt Fiber Sensors 2018;TuE100. https://doi.org/10.1364/OFS.2018.TuE100.
[33] Woon W, Ravindran PB, Ekayanake P, Lim YY, Khalid J. A study on the effect of detector resolution on gamma index passing rate for VMAT and IMRT QA. J Appl Clin Med Phys 2018;19:230–48. https://doi.org/10.1002/acm2.12285.
[34] Paganini L, Reggiori G, Stravato A, Palumbo V, Mancosu P, Lobefalo F, et al. MLC parameters from static fields to VMAT plans: an evaluation in a RT-dedicated MC environment (PRIMO). Radiat Oncol 2019;14:216. https://doi.org/10.1186/s13014-019-1421-y.
[35] Bergman AM, Gete E, Duzenli C, Teke T. Monte Carlo modeling of HD120 multileaf collimator on Varian TrueBeam linear accelerator for verification of 6X and 6X FFF VMAT SABR treatment plans. J Appl Clin Med Phys 2014;15:148–63. https://doi.org/10.1120/jacmp.v15i3.4686.
[36] Gasparian P, Vanhavere F, Yukihara E. Evaluating the influence of experimental conditions on the photon energy response of Al2O3: C optically stimulated luminescence detectors. Radiat Meas 2012;47:243–9. https://doi.org/10.1016/j.radmeas.2012.01.012.
[37] Lambert J, Yin Y, McKenzie DR, Law SH, Ralston A, Suchowerska N. A prototype scintillation dosimeter customized for small and dynamic megavoltage radiation fields. Phys Med Biol 2010;55:1115. https://doi.org/10.1088/0031-9155/55/4/014.
[38] Pönisch F, Archambault L, Briere TM, Sahoo N, Mohan R, Beddar S, et al. Liquid scintillator for 2D dosimetry for high-energy photon beams. Med Phys 2009;36:1478–85. https://doi.org/10.1118/1.3106390.
[39] Guillot M, Gingras L, Archambault L, Beddar S, Beaulieu L. Performance assessment of a 2D array of plastic scintillation detectors for IMRT quality assurance. Phys Med Biol 2013;58:4439. https://doi.org/10.1088/0031-9155/58/13/4439.